CARBON ISOTOPE STRATIGRAPHY AND DIAGENESIS OF PENNSYLVANIAN (DESMOINESIAN-MISSOURIAN) CARBONATES IN EAST-CENTRAL IDAHO

A Senior Scholars Thesis

by

STEPHANIE G. WOOD

Submitted to the Office of Undergraduate Research
Texas A&M University
in partial fulfillment of the requirements for the designation as

UNDERGRADUATE RESEARCH SCHOLAR

April 2011

Major: Geology

CARBON ISOTOPE STRATIGRAPHY AND DIAGENESIS OF PENNSYLVANIAN (DESMOINESIAN-MISSOURIAN) CARBONATES IN EAST-CENTRAL IDAHO

A Senior Scholars Thesis

by

STEPHANIE G. WOOD

Submitted to the Office of Undergraduate Research
Texas A&M University
in partial fulfillment of the requirements for the designation as

UNDERGRADUATE RESEARCH SCHOLAR

Approved by:

Research Advisors: Ethan Grossman,
Michael Pope

Director for Honors and Undergraduate Research: Sumana Datta

April 2011

Major: Geology

ABSTRACT

Carbon Isotope Stratigraphy and Diagenesis of Pennsylvanian (Desmoinesian-Missourian) Carbonates in East-central Idaho. (April 2011)

Stephanie G. Wood
Geology and Geophysics Department
Texas A&M University

Research Advisors: Dr. Ethan L. Grossman and Dr. Michael Pope
Geology and Geophysics Department

Carbon isotope stratigraphy of carbonate sediments is instrumental in examining major perturbations in the global carbon cycle and in correlating strata. However, the primary isotopic signal recorded in these sediments can vary with depositional environment and diagenetic alteration. This study examines the carbon isotope stratigraphy and its relation to depositional environment, lithology, and diagenetic history in a section of the 312-307 million year old Pennsylvanian (Desmoinesian-Missourian) Snaky Canyon Formation in the Beaverhead Mountains, east-central Idaho.

Petrography of 90 thin sections show carbonate rocks ranging from mudstone to boundstone containing variable amounts of eolian siliciclastics with as much as 50% silt to medium sand grains in some samples. The abundance of siliciclastic influx decreases upsection to less than 1% sand and roughly corresponds to an increase in parasequence thickness. Open marine carbonate facies include abundant crinoids, bryozoans, foraminifera, brachiopods, green algae, phylloid algae, and arthropod fragments. Chert,

bioturbation features (e.g. burrows), intraclasts, pellets, coarse calcite spar, calcite-filled fractures, and fossil silicification also occur in these rocks. Cathodoluminescence (CL) analysis of thin sections reveals a lack of luminescence in nearly all components, suggesting that depositional and diagenetic waters were low in Mn^{2+} or high in Fe^{2+}.

Approximately 130 billets were analyzed to yield $^{13}C/^{12}C$ and $^{18}O/^{16}O$ ratios. Fractures have much lower $\delta^{18}O$ (-13.9‰) reflecting post-depositional tectonic processes. Most of the isotopic data for micritic components are within -8 to -1‰ for $\delta^{18}O$ and -1 to +5‰ for $\delta^{13}C$. Previously reported oxygen isotope values for Pennsylvanian brachiopods from the U.S. Midcontinent are -2.2 ±0.7‰, indicating outlier $\delta^{18}O$ values in this study are altered. Most of the isotope data for carbon are within previously reported Pennsylvanian fine grained carbonate ranges of +1 to +5‰. These isotopic values appear to be independent of lithology and percent carbonate; thus, the main controlling influence on the $\delta^{13}C$ and $\delta^{18}O$ data may be depositional environment. Three significant trends in the $\delta^{13}C$ data appear to correspond to thickness and boundaries of stratigraphic parasequences. Isotope values in this study were compared to those of Arrow Canyon, Nevada and showed similar trends for the Desmoinesian but not for the Missourian.

ACKNOWLEDGMENTS

The author would like to thank Dr. Ethan L. Grossman and Dr. Michael Pope for their outstanding help and contribution to this research. Without their guidance, this paper would not have been possible. Thanks also go to M.S. candidate, Casey Jolley, for his amazing field efforts in collecting the samples and for his great help in preparing them for analysis. The author thanks Art Kasson for his part in isotope analysis and Dr. Ray Guillemette for use of his polishing equipment.

NOMENCLATURE

‰	Parts per thousand, or “per mil”
$\delta^{18}O$	Lower case delta ^{18}O to ^{16}O ratio that is normalized to VPDB (see Appendix, Equation 1)
$\delta^{13}C$	Lower case delta ^{13}C to ^{12}C ratio that is normalized to VPDB (see Appendix, Equation 2)
CL	Cathodoluminescence
DIC	Dissolved inorganic carbon = $(CO_2)_{aq} + HCO_3^- + CO_3^{2-}$
HMC	High magnesium calcite
HST	Highstand systems tract
IRMS	Isotope ratio mass spectrometer
LMC	Low magnesium calcite
m	Meters
Ma	Million years
pCO_2	Partial pressure of carbon dioxide, total amount of CO_2 in the atmosphere
TST	Transgressive systems tract
VPDB	Vienna Pee Dee Belemnite

TABLE OF CONTENTS

LIST OF FIGURES AND PLATES

CHAPTER I

INTRODUCTION

Application of isotopes for stratigraphy

When studying paleoclimate, geoscientists commonly use stable isotope stratigraphy to analyze perturbations in the ancient carbon and oxygen cycles and interpret major environmental changes in ancient Earth. Glaciations, temperature changes, changes in salinity, and changes in ocean chemistry and pCO_2 can be recorded as variations in carbon and oxygen isotopes in carbonate rocks (e.g., Grossman, 1994; Weissert et al., 2008; Mii et al., 1999, 2001; Saltzman, 2003; Buggisch et al., 2011). Carbon isotopes in particular can be useful in correlating widely spaced measured sections, if the original $\delta^{13}C$ signature is preserved and anomalies or large excursions are global in extent (e.g. the Valanginian-Hauterivian carbon isotope excursion) (Weissert et al., 2008). This study analyzed fine-grained carbonate rocks from the Snaky Canyon Formation in east-central Idaho to determine lithology, depositional environment, and percent carbonate to determine possible influences on carbon isotope stratigraphy.

The most reliable pre-Cenozoic marine carbon isotope signatures occur in pelagic bulk carbonates or unaltered fossils (Popp et al., 1986; Weissert et al., 2008). While it is desirable to develop carbon isotope stratigraphies for Paleozoic seas based on well preserved low magnesium calcite (LMC) fossils such as brachiopod shells (Weissert et

---

This thesis follows the style of Geology.

al., 2008, Buggisch et al. 2011), fine-grained carbonate matrix offers a high temporal resolution for global carbon cycle studies not available from fossils due to lack of preservation or abundance (Saltzman, 2005; Weissert et al., 2008). Thus, the general approach to carbon isotope stratigraphy in Paleozoic sediments is to analyze petrographically screened, fine-grained carbonate due to its facies-indiscriminant $\delta^{13}C$ records, stratigraphic continuity, and tendency toward providing a primary, non-diagenetic signal (Saltzman, 2005; Batt at al., 2007). Mesozoic and Cenozoic marine sediments are abundant, but because the sea floor is no older than 180 million years old, Paleozoic sediments are limited to those from continental margins and epicontinental seas which are biased toward interglacial intervals with high sea level (Grossman 2012).

Besides a lack of Paleozoic pelagic sediments, the use of $\delta^{18}O$ and $\delta^{13}C$ from fine-grained carbonate as stratigraphic tools has its limitations. Even if a major global event is recorded in the rock record, sometimes contrasting trends appear in the isotope record that may reflect local environmental change, making it difficult to identify causality and establish age constraints (Weissert et al., 2008). Additionally, diagenesis is a particular concern for Paleozoic sediments because cementation and recrystallization are likely to have affected these older rocks altering their original marine carbon isotope values (Weissert et al., 2008). Also, carbonates from basinal settings have lower $\delta^{13}C$ values than those from shallow water (Buggisch and Mann, 2004), so depositional environment can be a key factor in variations (Weissert et al., 2008). Lack of control for the source of carbonates (e.g. biogenic versus abiogenic, calcite, or aragonite) can also cause a

significant variation in $\delta^{13}C$ values by about 2‰ (Grossman, 1994). These many pitfalls have hindered an internationally accepted carbon isotope stratigraphic standard.

Factors controlling $\delta^{13}C$ of carbonate minerals

$\delta^{13}C$ of carbonate minerals depends on the isotopic composition of the dissolved inorganic carbon (DIC) of the solution in which the carbonate precipitates (Weissert et al. 2008). Local DIC $\delta^{13}C$ is affected by photosynthesis and respiration. Photosynthesis at the photic zone enriches the DIC in ^{13}C, while respiration in and below the photic zone releases light carbon and decreases $\delta^{13}C$ in the DIC (Grossman, 1994; Weissert et al., 2008). Higher $\delta^{13}C$ values in the global seawater DIC results from excess burial and preservation of organic carbon while a lower value can be produced from enhanced weathering of sedimentary organic carbon (Buggisch et al., 2011). The $\delta^{13}C$ of carbonate rocks can also be influenced by diagenesis. Lower $\delta^{13}C$ values signify interaction of the rock with $\delta^{13}C$-depleted meteoric waters, whereas higher $\delta^{13}C$ values can indicate the preservation of the primary $\delta^{13}C$ signal (Buggisch et al., 2011).

Mineralogy of carbonates can greatly determine the extent that diagenetic alteration affects the rock's isotopic values. In inorganic precipitation studies, Romanek et al. (1992), found that carbon isotope fractionation between aragonite and calcite was +1.7‰ and was independent of temperature. In naturally precipitated carbonates, aragonite can be on average 1‰ higher in $\delta^{13}C$ than high magnesium calcite (HMC) and

that HMC cements can be +0.2‰ enriched in $\delta^{13}C$ compared with LMC components in Holocene reefal carbonates (Gonzalez and Lohmann, 1985). This latter enrichment was attributed to carbon isotope fractionation associated with Mg substitution in calcite (Gonzalez and Lohmann, 1985). Thus, a drawback to bulk carbonate analysis is that the rocks may have originally consisted of different amounts of HMC, LMC, and aragonite, and may have higher $\delta^{13}C$ values than a sample originally composed of only LMC.

Vital effects, fractionation in isotopic compositions in an organism due to life processes, can lower $\delta^{13}C$ and $\delta^{18}O$ values for biogenic carbonates due to kinetic effects or preferential precipitation of metabolically derived carbon-oxygen compounds (Grossman, 1994). Habitat also influences isotopic composition. Increased paleodepths will likely yield lower $\delta^{13}C$ and higher $\delta^{18}O$ values due to a change from photosynthesis to respiration in dominant active processes (Grossman 1994). Additionally, different taxa (i.e. *Crurithyris* versus *Eridmatus* brachiopods) can exhibit different $\delta^{18}O$ and $\delta^{18}O$ values due to vital or microhabitat effects (Grossman, 1994).

While stable isotope stratigraphy is a useful tool for studying ancient global conditions, oxygen and carbon values can be altered by diagenesis, the physical and chemical changes that occur in sediments during lithification (McIlreath and Morrow, 1990). After deposition, sediments are subjected to a variety of diagenetic processes: compaction, cementation, mineral recrystallization from solution, solution leaching, organic degradation, and possibly the generation of hydrocarbons (McIlreath and Morrow,

1990). There generally are three environments for carbonate diagenesis: seafloor, meteoric, and deep burial. Seafloor diagenesis involves reactions with marine waters, meteoric diagenesis is controlled by freshwater and brackish waters, and deep burial diagenesis is influenced by geothermally-heated porewaters (James and Choquette, 1983a). These diagenetic environments can cause overprinting of the original primary carbon and oxygen isotope signals. A shift to more negative $\delta^{13}C$ and $\delta^{18}O$ values are generally characteristic of meteoric diagenesis because groundwaters have an average $\delta^{13}C$ of -10‰ due to interaction with isotopically light organic matter and typically several per mil lower than sea water for $\delta^{18}O$ (Hudson, 1977; Anderson and Arthur, 1983). Since diagenesis leads to chemically stable mineral phases like low magnesium calcite (LMC) (Grossman, 1994), isotopic compositions of LMC can survive for hundreds of millions of years, even after the rock has undergone multiple stages of diagenesis (James and Choquette, 1983b; Meyers and Lohmann, 1985). Although carbonate sediment can recrystallize and lithify during diagenesis (which is of concern for Paleozoic studies), the $\delta^{13}C$ of the micritic carbonates can be retained because the high inorganic carbon content of limestones buffers the $\delta^{13}C$ values from being altered (Grossman, 1994). Additionally, because fluids that interact with carbonates contain more oxygen (as water) than carbon (as DIC), $\delta^{13}C$ values are less likely than $\delta^{18}O$ to be affected by carbonate dissolution and reprecipitation (Hudson, 1977). In biologically active zones (i.e. soils), care must be taken to avoid exposure surfaces when sampling because oxidation of organic material will release ^{13}C-depleted carbon that may exchange with carbonate minerals in the rock (Grossman, 1994).

Oxygen isotope stratigraphy

Carbonate $\delta^{18}O$ depends on the temperature and isotopic composition of the fluid in which the rock precipitates, making $\delta^{18}O$ a proxy for seawater temperature (Weissert et al., 2008). However, lithified sediments that are diagenetically altered (such as those in this study) will preserve $\delta^{18}O$ values that are not primary. High sand content, like those in some samples in this study, can cause some carbonate rocks to be more permeable and experience larger carbon and oxygen fluxes (Grossman, 1994). Thus, because the focus of this study is carbon isotope stratigraphy and since meteoric diagenesis indicators are observed (see Results), $\delta^{18}O$ values are only examined as indicators of diagenesis and delimit the origin of diagenetic fluids.

Geologic setting of study

Location

The Snaky Canyon Formation is a 600-1200 m thick Pennsylvanian (Desmonesian-Missourian) carbonate-siliciclastic unit, approximately 306-309 million years (Ma) old. Outcrops of the study area are located in east-central Idaho near the Montana-Idaho border (Figure 1). This formation consists of three members: the Bloom Member, Gallagher Peak Sandstone, and the Juniper Gulch Member (Archuleta et al., 2006). The Snaky Canyon Formation overlies the Mississippian Bluebird Mountain Sandstone and is unconformably overlain by the Permian Phosphoria Formation (Archuleta et al., 2006; Figure 2). This study will focus on a 382 to 428 m interval in the Desmoinesian-

Missourian section of the Bloom Member. The Snaky Canyon Fo-rmation was deposited along an open marine coastline (Figure 3) offshore of the Quadrant-Tensleep Sandstone.

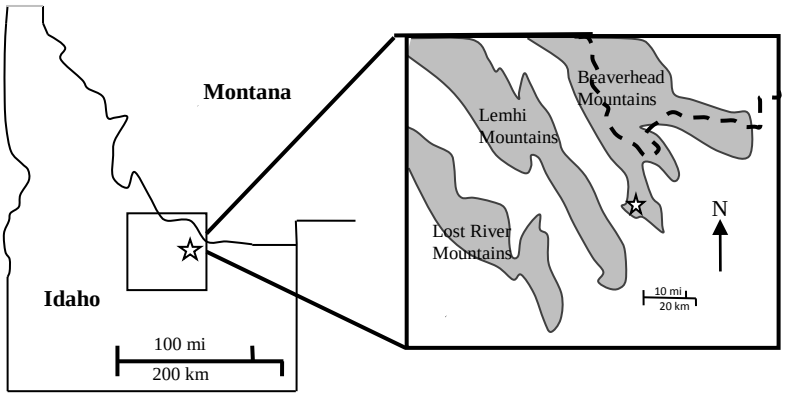

Figure 1: Location map for the Beaverhead Mountains. The star marks the location of the samples in this study. Approximately GPS coordinates 44.139156, -112.801913 (N 044 08' 20", W 112 48' 06").

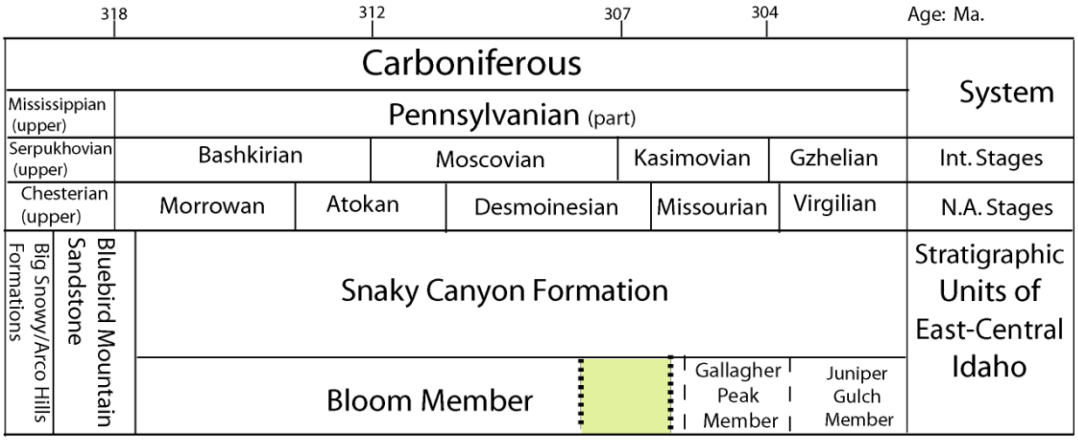

Figure 2: Carboniferous stratigraphy of east-central Idaho. The study interval is the Desmoinesian-Missourian Bloom Member interval of the Snaky Canyon Formation (highlighted in green). Data for figure from Archuleta et al., 2006 and Pope et al., 2008.

Depositional environment

Snaky Canyon's depositional environments are well documented (e.g. Archuleta et al., 2006; Skipp et al., 1979; Tremblay, 1996, Rankey, 1997) and were deposited on a gently sloping carbonate ramp in an open marine environment. These rocks record eolian to deep subtidal facies (Archuleta et al. 2006).

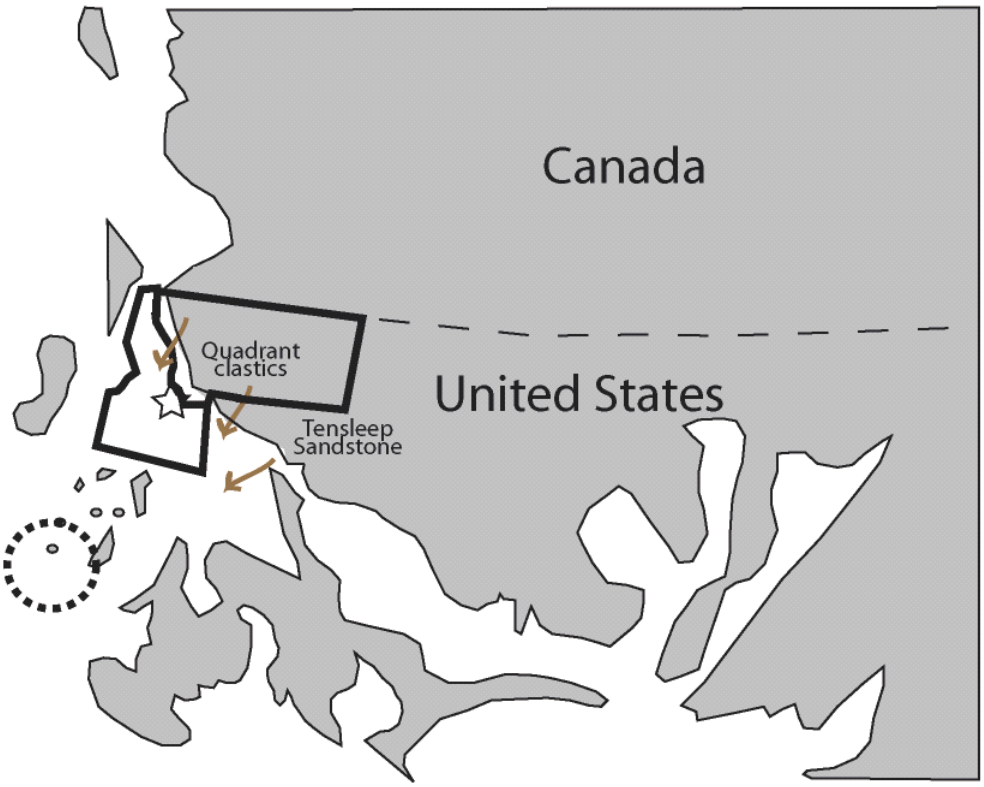

Figure 3: Approximate paleogeography of Western North America during the Late Paleozoic. Dotted circle shows approximate location of Arrow Canyon, star represents area for this study. Note that Snaky Canyon was in an open marine environment during this time. Map modified from Pope et al. (2008) and Blakey, R.C. (2005).

The lower part of Snaky Canyon Formation formed on a shallow water carbonate ramp above the Mississippian foreland deposits created by the Antler Orogeny (Skipp et al.,

1979). The upper part of the Snaky Canyon Formation was formed on a carbonate ramp protected from direct open ocean currents by the Copper Basin Highlands (Skipp et al., 1979). During deposition, as sea levels rose and fell due to glacial expansion and contraction, eolian siliciclastics equivalent to the Quadrant Formation in Montana and the Tensleep Sandstone Formation in Wyoming flooded the carbonate ramp (Archuleta et al., 2006; Tremblay, 1996). The Snaky Canyon Formation represents a 2nd-order depositional megasequence of a 10-15 million year transgression-regression cycle where high frequency sea level changes varied up to 16 m (Archuleta et al., 2006). The facies of the upper Snaky Canyon Formation were subdivided (Figure 4) into transgressive systems tract (TST) and highstand systems tract (HST) facies and these are similar to facies in the Bloom Member (Archuleta et al., 2006).

The transgressive systems tract (TST) (Figure 4) contains multiple facies (1 and 4a) characterized by predominantly detrital quartz that are interpreted to represent an eolian setting, beach or shoreface setting, and subtidal depositional environments, respectively. Facies 2b, 2c, 4a, and 5c are mixed carbonate-siliciclastic facies ranging from arid tidal flat, intertidal zones, lower shoreface setting, shallow subtidal setting, and nearshore shallow water subtidal depositional environments. Facies 5, 6, and 7 are carbonate-rich facies deposited in subtidal conditions within fair-weather wave base to deep subtidal below fair weather wave base.

Eight facies were identified within the highstand systems tract (HST) of the Snaky Canyon Formation (Figure 4). Depositional environments for mixed carbonate-siliciclastic facies are restricted to evaporite arid tidal flat, cryptalgalaminite deposition on a semi-arid tidal flat, and a protected landward lagoon. The carbonate-dominated facies are very similar or identical to the subtidal facies of the TST. The primary difference between TST and HST facies is the abundance of siliciclastic dominated facies in the TST and lack of these facies in the HST.

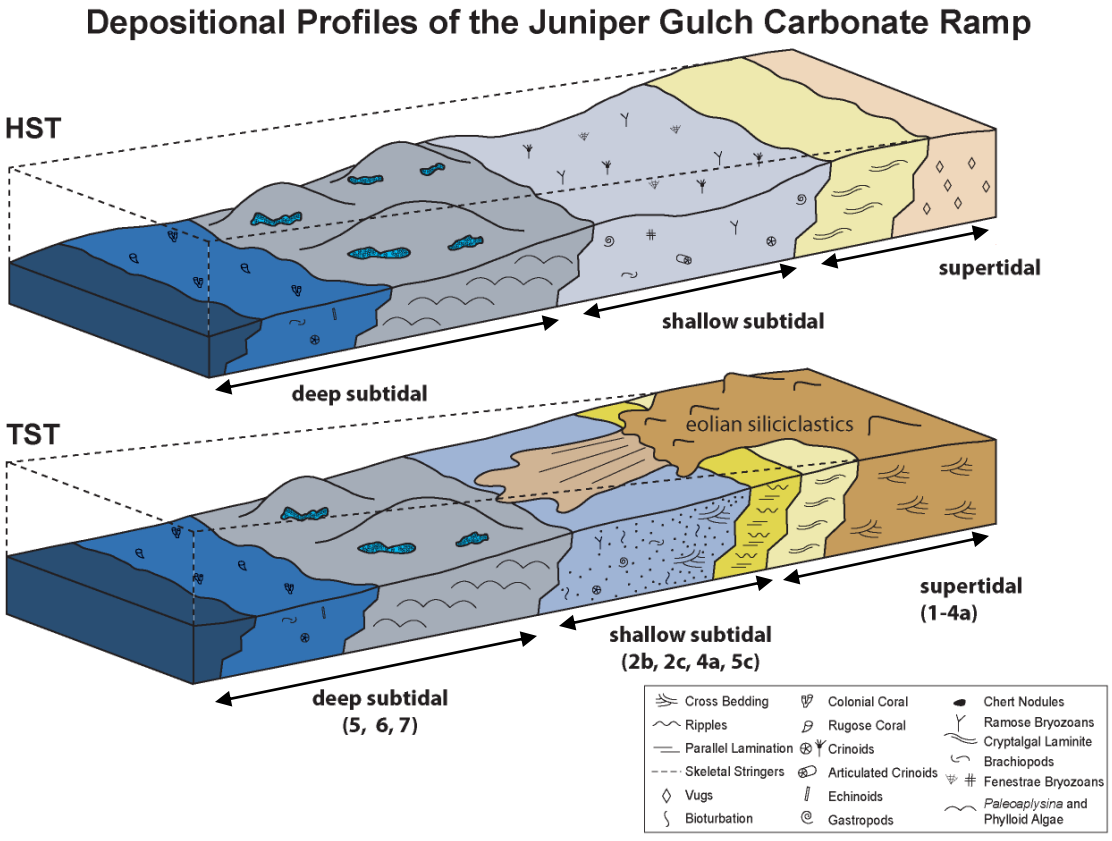

Figure 4: Illustration of Juniper Gulch depositional facies comparative to Snaky Canyon (modified from Archuleta et al. 2006).

Study objectives

Snaky Canyon's depositional environments are well-known, but little is understood about its carbonate-siliciclastic diagenesis and carbon stratigraphy. This study used petrography and isotope analysis to provide insights into carbon isotope stratigraphy and diagenetic conditions for the 328-482 meter interval of the Bloom Member of Snaky Canyon measured section in the Beaverhead Mountains (Pope et al., 2006). Snaky Canyon deposition occurred in an open marine setting, so its carbon isotope stratigraphy may provide a record for continental margins far from epicontinental seas. Our carbon isotope stratigraphy is compared to the nearest and most complete isotope stratigraphy, that from Arrow Canyon, Nevada to test for correlative $\delta^{13}C$ events. This information can be used to help construct a general global isotope curve for the Desmoinesian and Missourian and possibly correlate its carbon fluctuations with major environmental changes.

CHAPTER II

METHODS

Petrographic and isotopic analyses were performed on 135 carbonate rock samples collected in August 2010 by Casey Jolley for his M.S. thesis on chemostratigraphy of the Bloom Member in east-central Idaho. Billets (cubes of rock) were cut from 90 samples that were deemed of interest (i.e. allochem-bearing rocks rather than homogeneous mudstones), polished with 200 and 600 grade alumina grit, and sent to National Petrographic Services contract lab for thin-sections. Thin-sections were examined using a petrographic microscope and a cathodoluminescence (CL) microscope stage.

Petrographic and cathodoluminescence microscopy

The petrographic microscope analysis identified cement content, grain type and abundance, percent carbonate, and grain size according to the Dunham (1962) classification system for carbonates. Fossil abundances, chert or silicification, fracturing, bioturbation features, and intraclasts were also noted and are summarized in the stratigraphic column. Thin sections with significant fractures, calcite cement, packstone texture with obvious cement, changes in texture, or calcite nodules were selected for (CL) analysis. CL indicates different diagenetic zones based on the ratio of Mn^{2+} to Fe^{2+} content (Boggs and Krinsley, 2006). If Mn^{2+} concentrations are a certain degree greater than Fe^{2+} concentrations, a sample will exhibit luminescence as an electron beam excites the ions and causes the material to emit light (Boggs and Krinsley, 2006; Meyers, 1974). Alternatively, if Fe^{2+} is in a high enough concentration compared to Mn^{2+}, the sample's

luminescence will be quenched. The exact concentration of Mn^{2+} required for luminescence in iron-poor samples is unclear: some studies suggest 1 ppm Mn^{2+} will activate luminescence, while others report that 25 ppm of Mn^{2+} is the minimum (Boggs and Krinsley, 2006; Marshall et al., 1988; Budd et al., 2000). In Mn^{2+}-poor samples, at least 100 ppm of Fe is required for the quenching of CL when Mn is below 200 ppm (Budd et al. 2000). Oxic waters are low in Mn^{2+}, so CL is dull to no luminescence for cement and other grains that precipitated in seawater or diagenetic fluids (McIlreath and Morrow, 1990). Sampling areas on the billet that are considered unaltered based on CL, staining techniques and elemental analysis, can provide more reliable isotope values reflecting original seawater conditions during deposition (Popp et al., 1986).

Twenty-six thin sections selected for CL analysis were polished with 3 and 0.3 μm alumina polishing grit and cleaned by ultrasonication for one minute in distilled water. The thin sections were examined using a TECHNOSYN Model 8200 MKII cathodoluminoscope. The operating conditions for the luminoscope were a gun current of 200-300 mA and a voltage 10-15 kV under vacuum of 0.07- 0.05 torr. Digital photos in plane light (PL) and CL were taken with a Coolsnap-Pro_{cf} camera using exposure times of one second and 40 seconds for PL and CL photomicrographs respectively. Since there are no standard practices for CL analysis, the amount of luminescence and thus the effectiveness of using it as a diagenetic indicator can be affected by the operating conditions and exposure time.

Stable isotope analysis

All of the samples from Snaky Canyon were analyzed for $^{13}C/^{12}C$ and $^{18}O/^{16}O$ ratios using the Gas Bench automated gas handling system and the DeltaPlus Isotope Ratio Mass Spectrometer (IRMS) at the Stable Isotope Geosciences Facility in the College of Geosciences, TAMU. Billets that were thin-sectioned were ultrasonicated with ethanol and methanol to remove the cutting oil, and placed in a low temperature oven (70^oC) to dry overnight. All billets were then cleaned with 20% HCl for about 3-5 seconds to remove any dust or residues (i.e. Brand and Brenckle, 2001), rinsed with deionized, distilled water, and left to dry on a clean piece of aluminum foil overnight.

Carbonate was sampled by drilling via Servo drill press with a 1 mm carbide tipped drill bit in homogeneous areas with as small a grain size as possible. Areas with fractures, chert, and large skeletal grains were avoided. Large calcite-filled fractures were sampled to examine the conditions of vein formation. Estimates were made of the percent of carbonate drilled, for later comparison with isotopic values. The powdered samples were reacted with three drops of phosphoric acid at 70^oC using the Gas Bench. The gas produced from this reaction was transferred through a cryogenic water trap and the CO_2 was analyzed on the IRMS. Oxygen and carbon isotope data were reported in delta notation ($\delta^{13}C$, $\delta^{18}O$) versus VPDB (Vienna Peedee belemnite) standard using NBS-19 as a reference gas. The average standard deviation for $\delta^{13}C$ and $\delta^{18}O$ were 0.09‰ and 0.47‰, respectively. The poorer precision for $\delta^{18}O$ was due to analytical problems, but is small compared with the natural variability of the samples. Furthermore, oxygen

isotopic signatures of shallow marine carbonates are usually strongly altered by meteoric diagenesis (Weissert et al., 2008) and are more variable in higher latitude samples, such as in our section (Grossman, 2012).

Problem summary

By sampling portions of the rocks determined to be least altered based on thin section and CL analysis, the carbon isotope values from the Snaky Canyon Formation will represent original oceanic isotope values. These isotope data are compared with published values of other Pennsylvanian carbonate rocks (e.g. Saltzman, 2003) to determine similarities and differences in their trends with relation to diagenetic history and global carbon isotope stratigraphy.

CHAPTER III

RESULTS

Petrography

Petrographic microscope

Petrographic estimates of percent carbonate show that most of the samples range from 35-100% carbonate with an average of 83% (Figure 5).

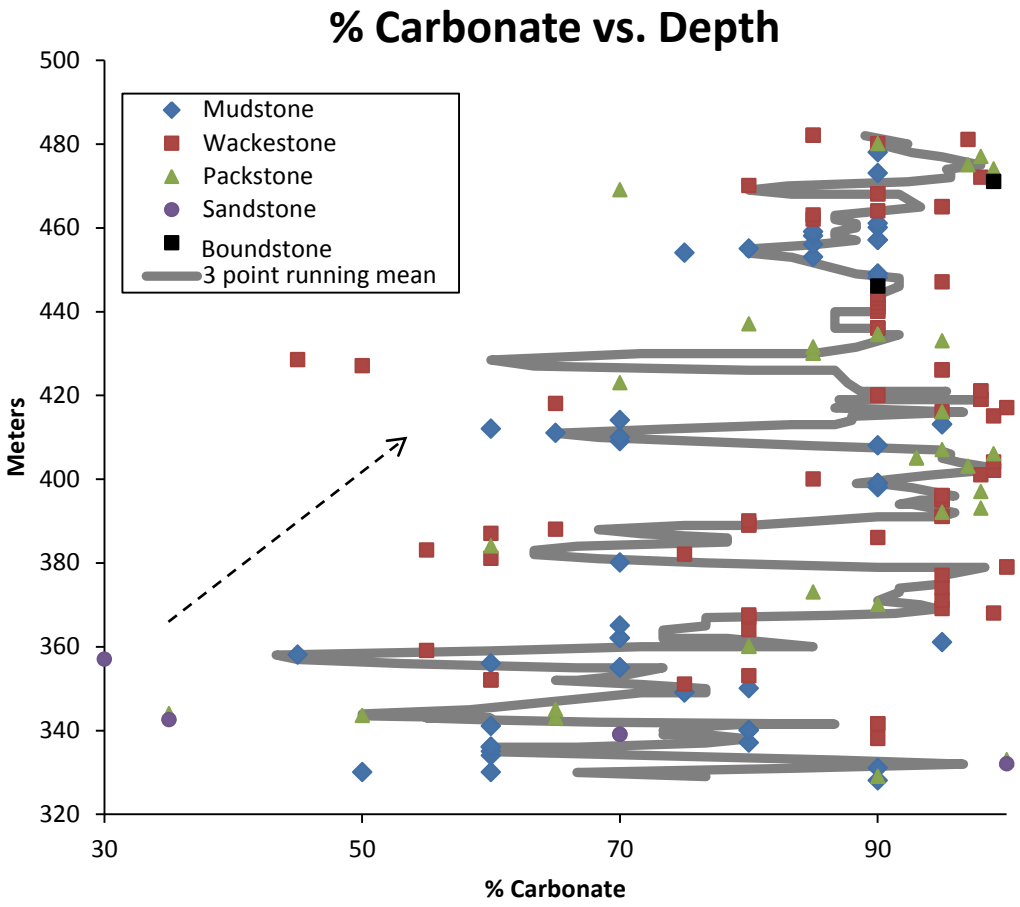

Figure 5: Percent carbonate based on petrographic analysis as a function of sample depth. Note how percent carbonate increases upsection in three episodes and siliciclastic input decreases.

The overall trend of the data shows three episodes of siliciclastic influx decreasing upsection. These episodes of increasing percent carbonate correspond roughly to upward increases in thickness of parasquences (Figure 6). The parasequence frequency appears to decrease upsection, and the average percent carbonate values appear to increase. Samples 99C through 144C in the uppermost part of the section (431.5- 482 m) show very few sand or silt grains. This overall reduction in silt and sand was suggested by Archuleta et al. (2006) to represent a decrease in the amplitude of glacio-eustatic sea level fluctuations in the Late Pennsylvanian, possibly in conjunction with the collapsing Gondwanan ice sheet (Isbell et al., 2003). Alternatively, the decrease in siliciclastic content may result from a shift in the wind direction or a southward migration of the Quadrant Sandstone (Archuleta et al., 2006).

Thin section examination under light microscope revealed abundant marine fossils including crinoids, bryozoans, brachiopods, foraminifera, green algae, phylloid algae, pelloids, and arthropod fragments. Rare ooids, chert nodules and intraclasts also are primary depostional features in these rocks. These features are characteristic of restricted subtidal to deeper subtidal facies (Archuleta et al. 2006). Chert replacement of allochems, calcitized evaporite nodules, calcite-filled fractures, and intraclasts also occur in the thin-sections and are indicative of diagenetic conditions. These features and fossil content were plotted on a stratigraphic column (Figure 6 and Appendix). By combining fossils, nodules , and rock type (Dunham classification), lithofacies in Figure 6 are subdivided into parasequences based on shallowing upward trends defined by Archuleta

et al. (2006) and Pope et al. (2008).The bottom of the section (328-358 m) has three parasequences with basal deep subtidal carbonate mudstones indicating a rapid sea level rise overlain by shallower carbonate facies capped by eolian siliciclastics that prograded onto the carbonate ramp (Archuleta et al., 2006). The middle part of the section (358 m to about 425 m) has parasequences that predominantly are fine-grained subtidal siliciclastic and carbonate bases recording rapid sea level rises, shallowing into skeletal wackestone and packstone produced during sea level falls (Archuleta et al., 2006). The mainly basal cherty, subtidal carbonate mudstone in these parasequences are overlain by bryozoan wackestones and packstones with crinoids and brachiopods characteristic of shallow subtidal facies (Archuleta et al., 2006). The uppermost part of the section (425-482 m) has multiple parasequences that are relatively thicker and contain phylloid algal layers that formed during rapid sea level rise and fall (Rankey, 1997). In the studied interval, there is a decrease in siliciclastic content upsection coincident with an upward thickening of parasequences and the initial occurrence of phylloid algae.

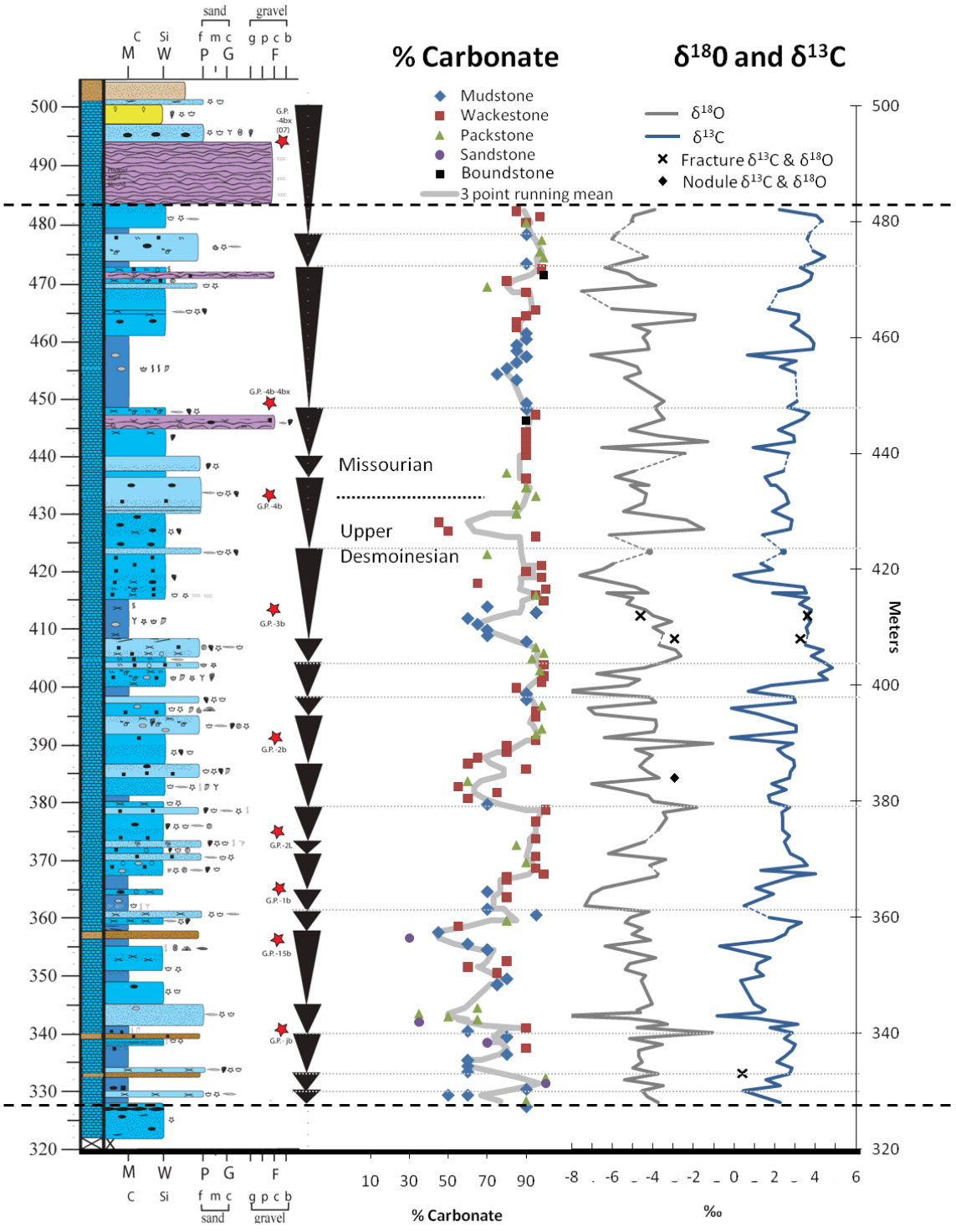

Figure 6: Stratigraphic column of Snaky Canyon with parasequences and percent carbonate compared to isotopic data. Dashed lines mark the study interval and black triangle represent parasequences shallowing upwards. The studied section begins 70 m above the Desmoinesian-Atokan boundary. The Upper Desmoinesian starts at 365 m. Stratigraphic column and parasequences are modified from Pope et al. (2008). See Appendix for a higher resolution stratigraphic column with complete legend and approximate unit locations.

Cathodoluminescence

Plane light microscopy show extensive diagenesis with abundance of calcite-filled fractures and chert replacing skeletal grains (especially brachiopods and crinoids). Such diagenetic features often exhibit cathodoluminescence because of Mn^{2+} added during reducing conditions in burial diagenesis (Boggs and Krinsley, 2006). In the Snaky Canyon samples, however, none of these features show significant luminescence except in sample 60C (Plate 1 and Plate 2). Most of the samples were dull to non-luminescent. Even after digital enhancement of images (increase of brightness and contrast by +40%), very few samples showed an improvement in CL brightness. This implies that the depositional and diagenetic waters were low in Mn^{2+} or high in Fe^{2+} (Batt et al., 2007; Meyers and Lohmann, 1985). The presence of Fe can quench luminescence, and is likely in these samples.

Sample 60C shows significant sector zoning cathodoluminescence in rhombohedral dolomite cements (Plate 2). This indicates that there were rapid porewater chemistry fluctuations during deposition of the secondary calcite in the vuggy wackestone. Sample 6C has a large calcite-filled fracture that did not luminesce. The vuggy wackestone in sample 71C was also dull or non-luminescent. Lastly, sample 26C contains a brachiopod shell which is nonluminescent. Normally, the lack of CL is used as an indicator of preservation, but as pointed out in Grossman (1994), if diagenetic calcite is not luminescent, CL cannot be used as an indicator of diagenesis.

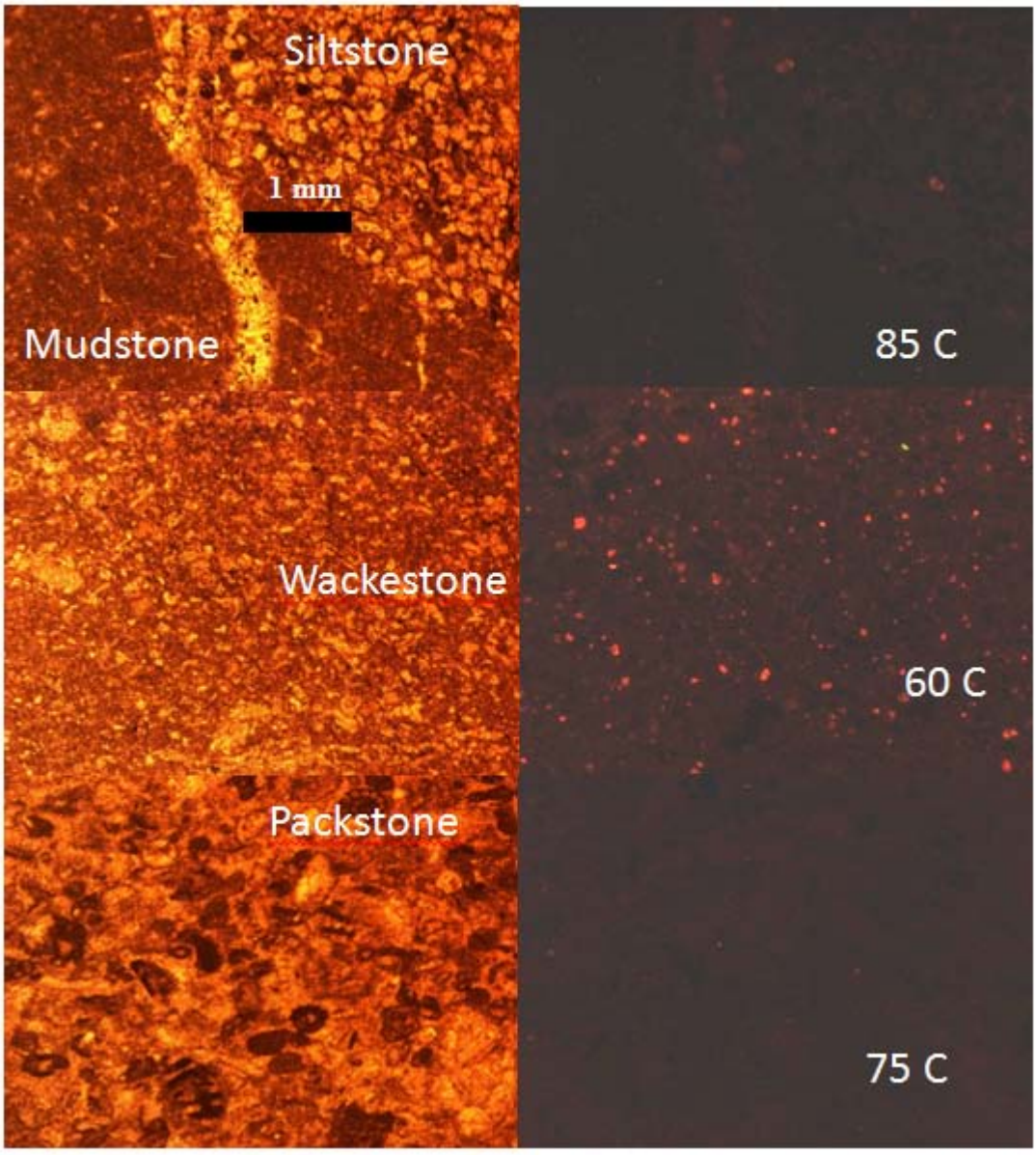

Plate 1: Representative PL (left), CL (right) micrographs of each major lithology in the study. Note the generally non-luminescent characteristics of each sample. Field of view is 3.19mm. CL photos were enhanced by adding +40% brightness and contrast.

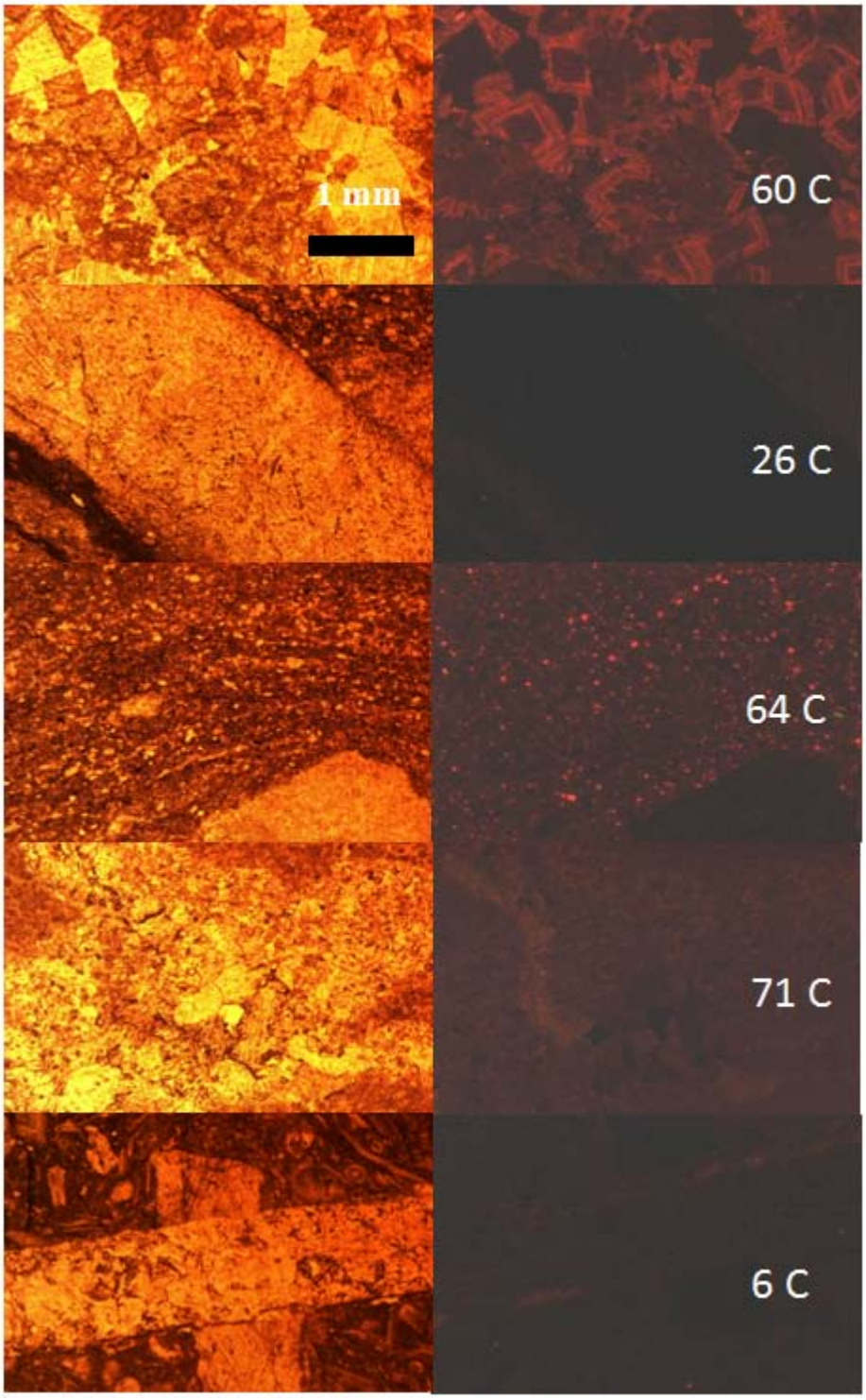

Plate 2: CL results from various samples. Photos on the left are in plane light; photos on the right are in CL. Sample 60C showed the greatest amount of luminescence, while most of the samples appeared non-to-slightly luminescent like 26C, 71C, and 64 C. Most notably, the calcite fracture in 6C and the calcite nodule in 64C (bottom right) did not luminesce.

Stable isotope results

The stable isotope results listed in the Appendix are plotted with the Snaky Canyon stratigraphic column in Figure 6. Oxygen isotope values vary from -8 to -1‰ and average -5‰. These values fall within previously reported ranges for Pennsylvanian fine-grained carbonates from North America (-7 to 0‰ Saltzman, 2003; M. Saltzman, pers. comm) but exhibit a wider range than Pennsylvanian brachiopods from North America (-1 to -4‰, Mii et al., 1999). Carbon and oxygen isotope values covary (Figure 6) which is often used as an indicator of meteroic diagenesis (Grossman, 1994). However, this covariance is weak in the Snaky Canyon data set and can also be caused by environmental factors.

There are three recognizable trends in the carbon isotope data (Figure 7). First, samples from 328-398 m show fairly consistent values averaging 2.5‰ and fluctuate between 1 and 3‰. These $\delta^{13}C$ values are within the range for bulk Pennsylvanian carbonate of +1 to +5‰ (Saltzman, 2003). A major excursion to higher $\delta^{13}C$ values (+3.5 to +4.8‰) occurs from 400-416 m. The values for this interval correspond to an increase in percent carbonate and a relatively thick subtidal parasequence. Finally, an increasing $\delta^{13}C$ trend from +2 to +4‰ is shown from 416-482 m (Figure 7) and the linear regression model (Figure 8) shows a clear increase of 2‰ with statistically significant correlation (Fisher and Yates, 1963). This increasing trend roughly correlates to thicker parasequences dominated by subtidal carbonate facies with decreased siliciclastic input (Figure 6).

Though some of the parasequence boundaries correspond to isotope peaks, the relationship between the boundaries and isotope signals is unclear.

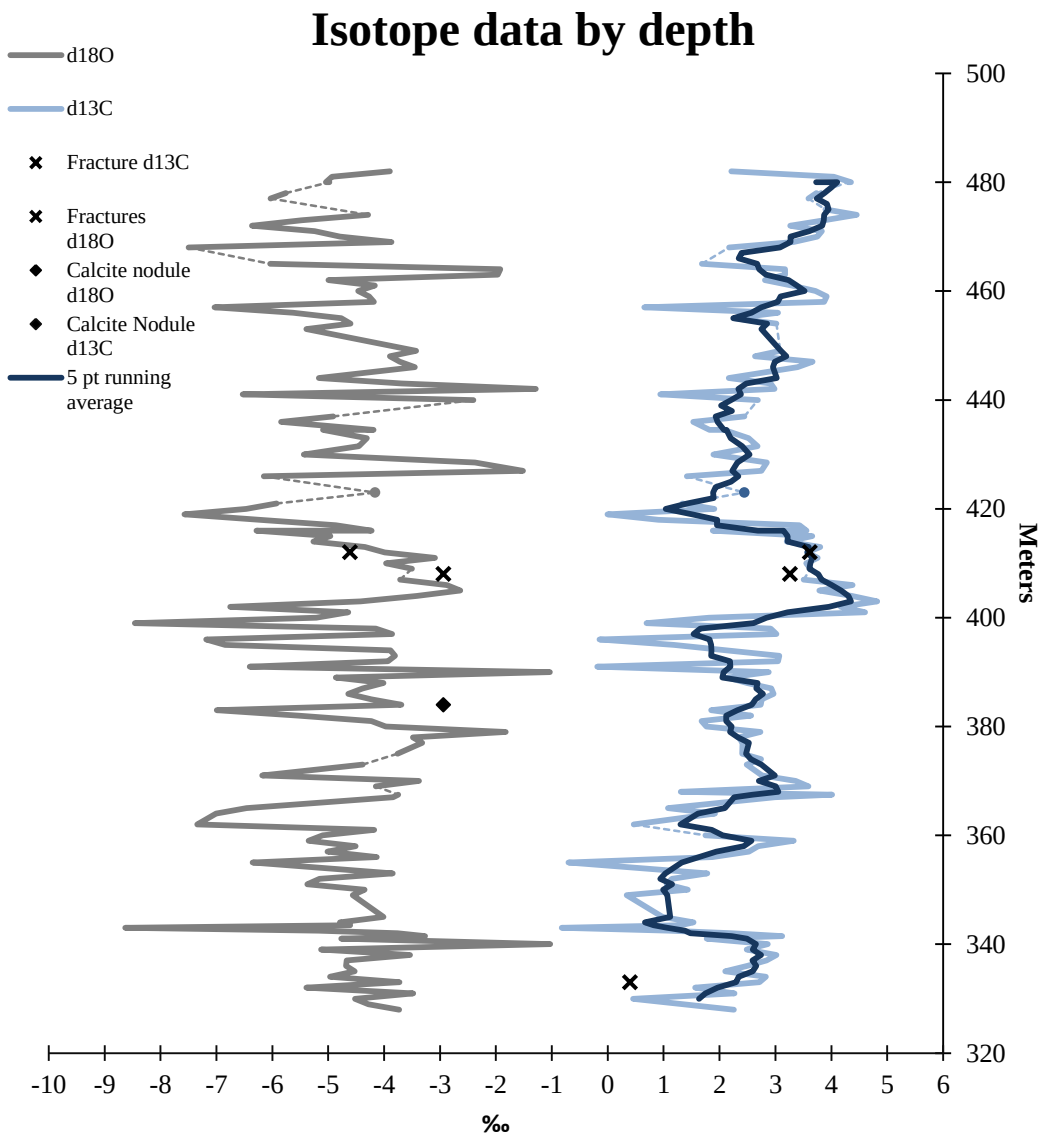

Figure 7: Isotope data by depth. The darker blue curve shows the five-point running mean of the $\delta^{13}C$ data.

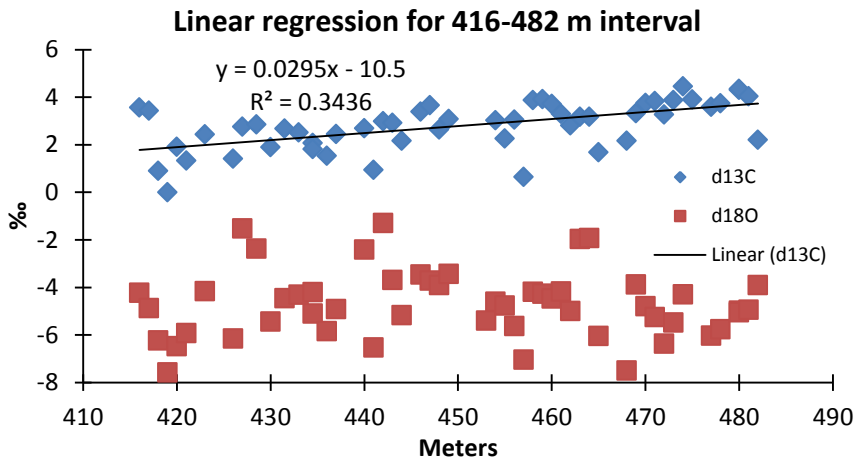

Figure 8: Linear regression for the third trend in the 416-482 m section of Snaky Canyon carbon isotope stratigraphy. The R value (0.5862) falls within the statistically significantrange for the number of data points (Fisher and Yates, 1963), indicating that the range for carbon isotopes is geniunely 1.9 to 4‰.

The carbon isotope signature from this study are suggested to be a primary marine signal due to petrography and CL results values and isotope values within previously reported Desmoinesian-Missourian ranges. $\delta^{13}C$ of carbonates deposited in subtidal settings waters should be more resistant to early diagenesis because cementation occurs in marine pore waters (Buggisch, et al. 2011). However sea-level lowstands can reduce carbonate deposition and meteoric diagenesis can alter the initial $\delta^{13}C$ value of the platform carbonates. (Buggisch et al., 2011).

The calcite fracture in 6C is non-luminescent in CL (Plate 2) with average $\delta^{18}O$ and $\delta^{13}C$ value of -13.7 ‰ and 0.4‰ respectively (N=2). These values are much lower than those of the surrounding matrix, and likely indicate that these fractures were formed and filled in association with later tectonic processes. These calcite veins exhibit isotopic

signatures similar to those of veins in the Wyoming Absaroka thrust sheet (Budai and Wiltschko, 1987). $\delta^{18}O$ values in the Absaroka veins were very low (-10.0 to -18.0‰), while bulk rock values were within -2 to -4‰. $\delta^{13}C$ values were very similar to the host rock (+3 to +6‰), a similar phenomenon that occurred in Snaky Canyon sample 6C (2.7 vs. 0.4‰ for $\delta^{13}C$ fine-grained vs. vein cement, respectively; and -3.7 vs. -13.7‰ for $\delta^{18}O$ fine-grained vs. fracture, respectively). The fractures in the Wyoming rocks were interpreted to record changing fluid compositions during thrusting, with temperatures estimated to range from 125 to 300^{o}C (Budai and Wiltschko, 1987). Because a similar low $\delta^{18}O$ occurred in fractures compared to bulk rock occurred in the Snaky Canyon samples, this suggests a warm, large-scale fluid migration thorough the Snaky Canyon rocks.

To determine if lithology affected isotopic composition, $\delta^{13}C$ was plotted versus $\delta^{18}O$ and keyed according to lithology (Figure 9). Note the positive correlation between carbon and oxygen isotopes discussed previously. Such a correlation may reflect a direct linkage between oxygen and carbon isotopic compositions, with lower values outside those reported for the Desmoinesian likely being diagenetically altered. The isotopic values of packstones clustered in a narrow range with only minor exception ($\delta^{18}O$ of -6 to -3‰ and $\delta^{13}C$ of 1 to 5‰), whereas wackestones varied more and showed outliers with lighter oxygen and carbon isotope values (-8 to -1‰ for $\delta^{18}O$ and 0 to +5 for $\delta^{13}C$). Mudstones also showed variability with $\delta^{13}C$ and $\delta^{18}O$ values of 0 to +4‰ and -8 to -

3‰. It is interesting that the packstone isotope data were higher in $\delta^{13}C$ and $\delta^{18}O$. Lower values for packstone relative to mudstone and wackestone might be expected because packstone is by definition coarser grained and has higher porosity and permeability than mudstones or wackestones, so diagenetic fluids would be expected to have greater influence on a packstone sample. The implications of this are not clear, but may have to do with early precipitation and cementation on the seafloor. With early cementation, packstone pores would be filled early losing permeability, meaning that later diagenetic fluids would be less likely to enter the rock and allow them to retain more of their primary isotope values. Though the packstone vales differ slightly from the mudstone and wackestone values, sufficient scatter in the $\delta^{13}C$ and $\delta^{18}O$ data indicate that lithology is not a main control on isotopic signature, similar to a chemostratigraphic study of findings of underlying Mississippian rocks (Batt et al., 2007).

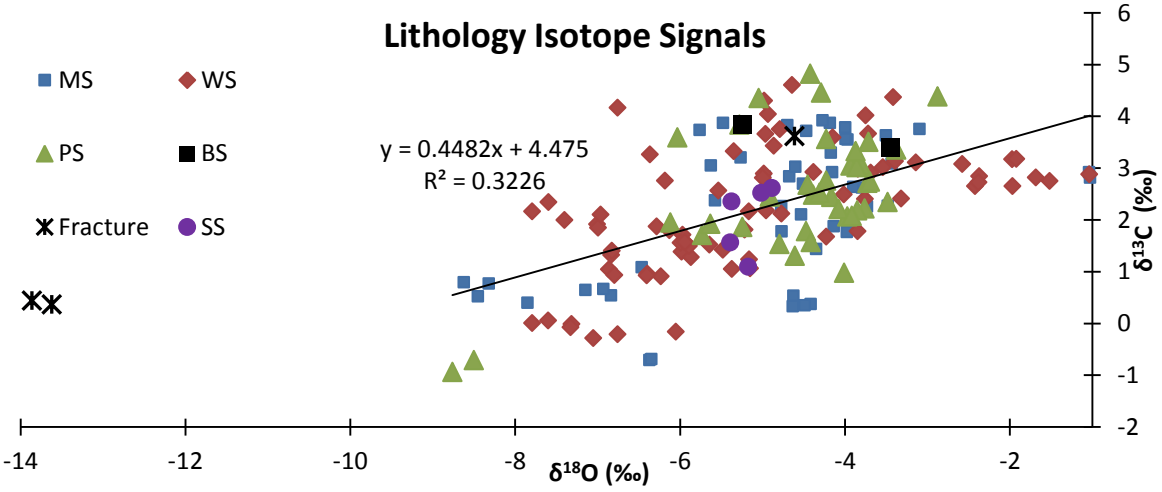

Figure 9: Oxygen and carbon isotope values plotted according to lithology. Values tend to be clustered together within previously reported ranges from Desmoinesian bulk carbonates (+1-5‰ for $\delta^{13}C$ and -7 to 0‰ for $\delta^{18}O$ in brachiopods, Saltzman 2003) MS = mudstone, WS = wackestone, PS = packstone, BS = boundstone, and SS = siltstone. R = 0.5680, a statistically acceptable level of significance (Fisher and Yates, 1963).

Because lithology and percent carbonate do not significantly influence these $\delta^{13}C$ and $\delta^{18}O$ values, the trends seen in the isotopic data likely reflect the primary isotopic signal. The carbon isotope stratigraphy of the Bloom Member was compared with an isotope stratigraphy of similar age in the Bird Spring Formation at Arrow Canyon, NV (Saltzman, 2003). These are the nearest and best data available for the western US and provide a test for primary trends and data validity (Figure 10). Because age constraints from conodont zonation were not available for the Snaky Canyon Formation, the isotopic data were fit to the Saltzman data by matching major isotope trends and excursions. Based on the $\delta^{13}C$ increase around 306.8 Ma, and the subsequent drop after 306 Ma, Snaky Canyon isotope values may be correlative with the Arrow Canyon data for the Desmoinesian, but not for the Missourian. The Snaky Canyon data only partially cover the Missourian and have been shown have an increasing trend (Figure 10). Arrow Canyon data cover the entire Missourian and show a decreasing trend in values. The reason for this incongruity is unclear, and better age constraints will allow a more definitive comparison between the $\delta^{13}C$ stratigraphies of these two western U.S. sections.

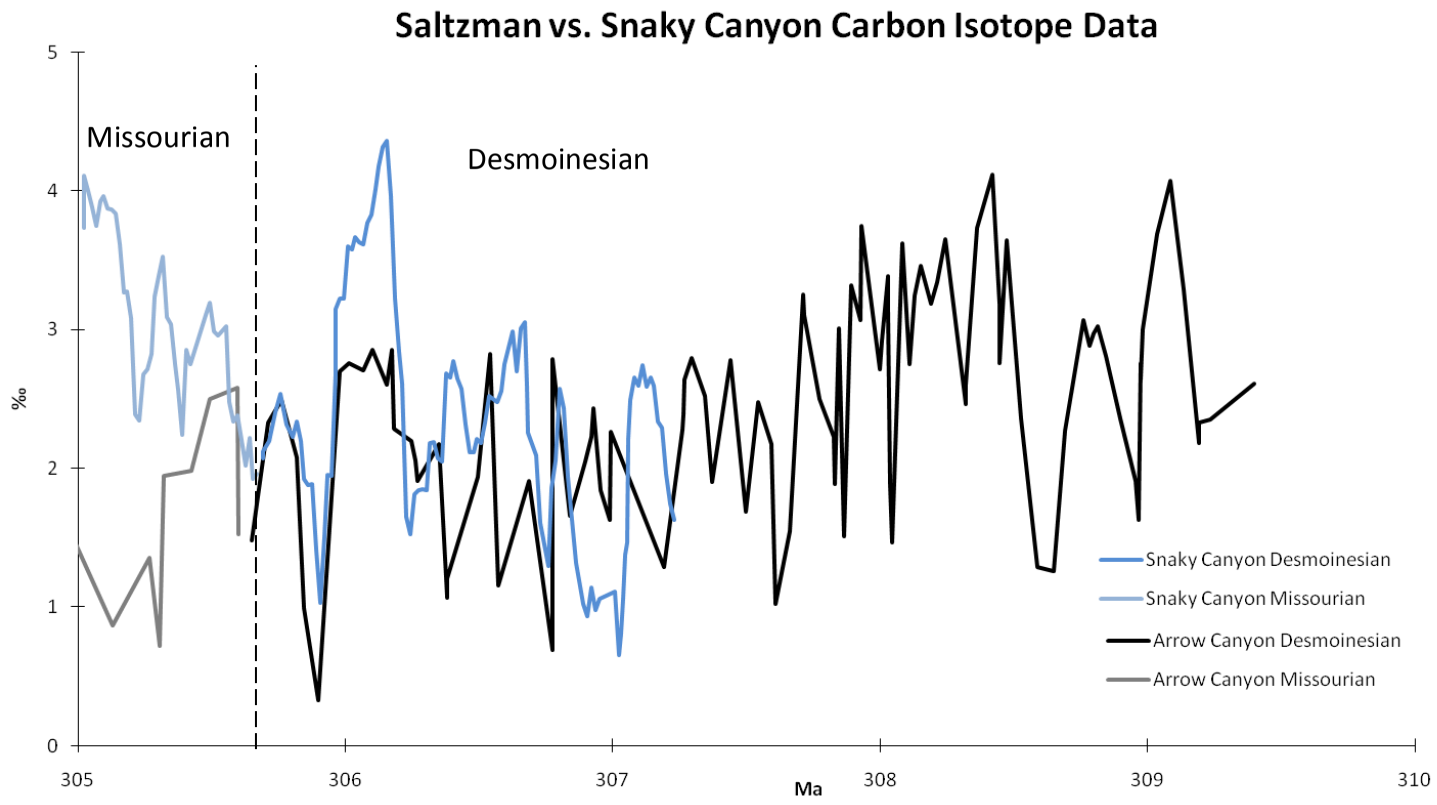

Figure 10: Comparison of Desmoinesian-Missourian carbon isotope stratigraphies for the Bird Spring Formation at Arrow Canyon, NM (Saltzman, 2003) and the Snaky Canyon Formation (5 point running average). Major excursions and trends in carbon isotopes were used to correlate together data.

CHAPTER IV

SUMMARY AND CONCLUSIONS

The goal of this study was to provide information on the carbon isotope stratigraphy and diagenetic history of Snaky Canyon Formation. Petrographic analysis shows fossils characteristic of open marine facies and a decreasing amount of silt and sand upsection. Lack of cathodoluminescence in nearly all components showed that porewaters were low in Mn^{2+} and (or) high in iron. Fine-grained carbonates varied from +1-5‰ for $\delta^{13}C$ and -8 to -1‰ for $\delta^{18}O$. In contrast, a calcite nodule had a very low $\delta^{13}C$ value (-19‰), reflecting precipitation in fluids influenced by oxidation of organic matter, probably in association with sulfate reduction, and a fracture had low $\delta^{18}O$ values (-13.7‰) suggesting formation at higher temperatures. Lithology and percent carbonate did not have a major effect on $\delta^{13}C$ and $\delta^{18}O$, but there was a positive correlation between oxygen and carbon isotopes, with lower values indicating diagenetic alteration. The Snaky Canyon carbon isotope stratigraphy has some features in common with the Desmoinesian and Missourian data for the Bird Spring Foramtion at Arrow Canyon, Nevada. Unfortunately, more defined biostratigraphic information is unavailable to refine this correlation further. Nevertheless, the similarity in the values and trends suggests that the original seawater $\delta^{13}C$ are reflected in the carbonate isotopic data and can be considered to be the primary isotopic trends for the Desmoinesian in the Bloom Member of Snaky Canyon.This information will help define the chemostratigraphy and depositional and diagenetic conditions of Pennsylvanian rocks in east-central Idaho.

REFERENCES CITED

Anderson, T.F., and Arthur, M.A., 1983, Stable isotopes of oxygen and carbon and their application to sedimentologic and paleoenvironmental problems, *in* Arthur, M.A., Anderson, T.F., Kaplan, I.R., Veizer, J. and Land, L.S., eds., Stable Isotopes in Sedimentary Geology, SEPM short course #10, Dallas 1983. Tulsa, Oklahoma: Society of Economic Paleontonologists and Mineralogists, p. 1-130.

Archuleta, B.J., Pope, M.C., Isaacson, P.E., Tremblay, M. L., Webster, G.D., 2006, Pennsylvanian cycles in east-central Idaho: a record of sea-level fluctuations on the western margin of Laurentia: The Mountain Geologist, v. 43, no. 2. p. 93-114.

Batt, L.S., Montanez, J.P., Isaacson, P., Pope, M.C., Butts, S.H., and Abplanalp, J., 2007, Multi-carbonate component reconstruction of mid-Carboniferous (Chesterian) seawater $\delta^{13}C$: Palaeogeography, Palaeoclimatolgoy, Palaeoecology, v. 256, p. 298-318.

Blakey, R., 2005, Paleogeography and geologic evolution of ancestral Rocky Mountains, Geological Society of America Annual Meeting, Salt Lake City, October, 2005.

Boggs, S., Krinsley, D., 2006, Application of Cathodoluminescence Imaging to the Study of Sedimentary Rocks: New York, Cambridge University Press, p.113-125.

Brand, V., and Brenckle, P., 2001, Chemostratigraphy of the Mid-Carboniferous boundary global stratotype section and point (GSSP), Bird Spring Formation,

Arrow Canyon, Nevada, USA: Palaeogeography, Palaeoclimatology, Palaeoecology, v. 165, p. 321-347.

Budai, J.M., Wiltschko, D.V., 1987, Structural controls on syntectonic diagenesis within the Haystack Peak region of the Absaroka thrust sheet, Idaho-Wyoming-Utah thrust belt, Thirty-Eighth Field Conference, in Wyoming Geological Association Guidebook, p.55-68.

Budd, D.A., Hammes, U, Ward W.B., 2000, Cathodoluminescence in calcite cements: new insights on Pb and Zn Sensitizing, Mn Activation, and Fe quenching at low trace-element concentrations, Journal of Sedimentary Research, Section A: Sedimentary Petrology and Processes, v. 70 (2000), no. 1., p. 217-226.

Buggisch, W., and Mann, U., 2004, Carbon isotope stratigraphy of Lochkovian to Eifelian limestones from the Devonian of Southern Europe, International Journal of Earth Sciences, v. 93, p. 521-541.

Buggisch, W., Wang, X., Alekseev, A.S., Joachimski, M. M., 2011, Carboniferous-Permian carbon isotope stratigraphy of successions from China (Yangtze platform), USA (Kansas) and Russia (Moscow Basin and Urals): Palaeogeography, Palaeoclimatology, Palaeoecology, v. 301, p. 18-38.

Dunham, R. J., 1962, Classification of carbonate rocks according to depositional texture. *in* Ham, W. E. (ed.), Classification of Carbonate Rocks: Tulsa. American Association of Petroleum Geologists Memoir, p. 108-121.

Fisher, R.A., and Yates, F, 1963, Statistical table for Biological, Agricultural, and Medical Research: London, Oliver and Boyd, 6th ed., p. 63.

Gonzalez, L.A., Lohmann, K,C., 1985, Carbon and oxygen isotopic composition of Holocene reefal carbonates, Geology, v. 13, p. 811-814.

Grossman, E.L., 1994, The carbon and oxygen isotope record during the evolution of Pangea: Carboniferous to Triassic, *in* Klein, G.D., ed., Pangea: Paleoclimate, Tectonics, and Sedimentation During Accretion, Zenith, and Breakup of a Supercontinent: Boulder, Colorado, Geological Society of America Special Paper 288, p. 207-228.

Grossman, E.L., 2012, Oxygen isotope stratigraphy, Oxygen isotope stratigraphy *in* Gradstein, F.M., Ogg, J.G., Smith, A., eds., A New Geologic Time Scale, Cambridge University Press (in press).

Hudson, J.D., 1977, Stable isotopes and limestone lithification, Journal of the Geological Society of London. v. 133, p 637-660.

Isbell, J.L., M.F. Miller, K.L. Wolfe, and P.A. Lenaker, 2003, Timing of late Paleozoic glaciations in Gondwana; was glaciations responsible for the development of Northern Hemisphere cyclothems?: *in* Chan, M.A. and Archer, A.W., eds., Extreme Depositional Environments; Mega End members in Geologic Time, GSA Special Paper 370, p. 5-24.

James, N.P. and Choquette, P.W., 1983a, Limestones: Introduction *in* I.A. McIlreath and D.W. Morrow, eds., Diagenesis, Geoscience Canada, reprint series 4, p. 9-13.

James, N.P. and Choquette, P.W., 1983b Limestones: The Sea Floor Diagenetic Environment *in* I.A. McIlreath and D.W. Morrow, eds., Diagenesis, Geoscience Canada, reprint series 4, p. 13-30.

Marshall, D.J., Giles, J.H., Marino, A., 1988, Combined instrumentation for EDS elemental analysis and cathodoluminescence studies of geological materials, *in* Hagni, E.D. (ed.), Process Mineralogy VI, Warrendale, Pennsylvania, The Metallurgical Society Inc, p. 35-117.

McIlreath I. A. and Morrow, D.W., 1990, *Diagenesis*, Geoscience Canada, reprint series 4. p 1-12.

Meyers, W.J., 1974, Carbonate cement stratigraphy of the Lake Valley Formation (Mississippian) Sacramento Mountains, New Mexico, Journal of Sedimentary Petrology, v. 44, no. 3, p. 837-861.

Meyers, W.J., and Lohmann, K.C., 1985, Isotope geochemistry of regionally extensive calcite cement zones and marine components in Mississippian limestones, New Mexico: *in* Schneiderman, N., and Harris, P.M., eds., Carbonate Cements, Society for Sedimentary Geology, Special Publication 36, p. 223-239.

Mii, H.S., Grossman, E.L., and Yancey, T.E., 1999, Carboniferous isotope stratigraphies of North America: Implications for Carboniferous paleoceanography and Mississippian glaciations: Geological Society of America Bulletin, v. 111, p. 960-973.

Mii, H.S., Grossman, E.L., Yancey, T.E, Chuvashov, B., and Egorov, A., 2001, Isotope records of brachiopod shells from the Russian Platform – Evidence for the onset of Mid-Carboniferous glaciations: Chemical Geology, v. 175, p. 133-147.

Pope, M.C., Abplanalp, J., and Isaacson, P.E., 2008, Eustatic variations within a Mississippian-Pennsylvanian subtidal mixed carbonate-siliciclastic succession, Beaverhead Mountains, Idaho-Montana: Poster

Popp, B. N., Anderson, T. F., and Sandberg, P. A., 1986, Brachiopods as indicators of original isotopic compositions in some Paleozoic limestones: Geological Society of America Bulletin, v. 97, p. 1262-1269.

Rankey, E.C., 1997, Relations between relative changes in sea level and climate shifts: Penn – Permian mixed carbonates – siliciclastics strata, western US, Geological Society of America Bulletin, v. 109, p. 1089-1100.

Romanek, C.S., Grossman, E.L., Morse, J.W., 1992, Carbon isotope fractionation in synthetic aragonite and calcite: effects of temperature and precipitation rate, Geochemica et Cosmochimica Acta, v. 56, p. 419-430.

Saltzman, M.R. 2003, Late Paleozoic Ice age: ocean gateway or pCO_2?: Geology, v. 31, p. 151-154.

Saltzman, M.R. 2005, Phosphorus, nitrogen, and the redox evolution of the Paleozoic oceans, Geology, v. 33, no. 7, p. 573–576.

Skipp B., Sando, W.J., and Hall, W.E., 1979, The Mississippian and Pennsylvanian (Carboniferous) Systems in the United States-Idaho, USGS Professional Paper 1110-AA, p. AA1-AA42.

Tremblay, M.L., 1996, Depositional controls on the Pennsylvanian-Permian Snaky Canyon carbonate platform, east-central Idaho [MS Thesis], Moscow, University of Idaho.

Weissert, H., Joachimski, M., Sarnthein, M., 2008, Chemostratigraphy, Newsletter of. Stratigraphy. v. 42 no.3, p. 145-179.

APPENDIX

Equations

To calculate isotope ratios (from Grossman 2002 and Grossman 1999)

$$\delta^{18}O \text{ ‰} = \frac{^{18}O/^{16}O_{sample} - {}^{18}O/^{16}O_{standard}}{^{18}O/^{16}O_{standard}} \text{ x } 1000 \quad \text{.....(1)}$$

$$\delta^{13}C \text{ ‰} = \frac{^{13}C/^{12}C_{sample} - {}^{13}C/_{12}C_{standard}}{^{13}C/^{12}C_{standard}} \text{ x } 1000 \quad \text{.....(2)}$$

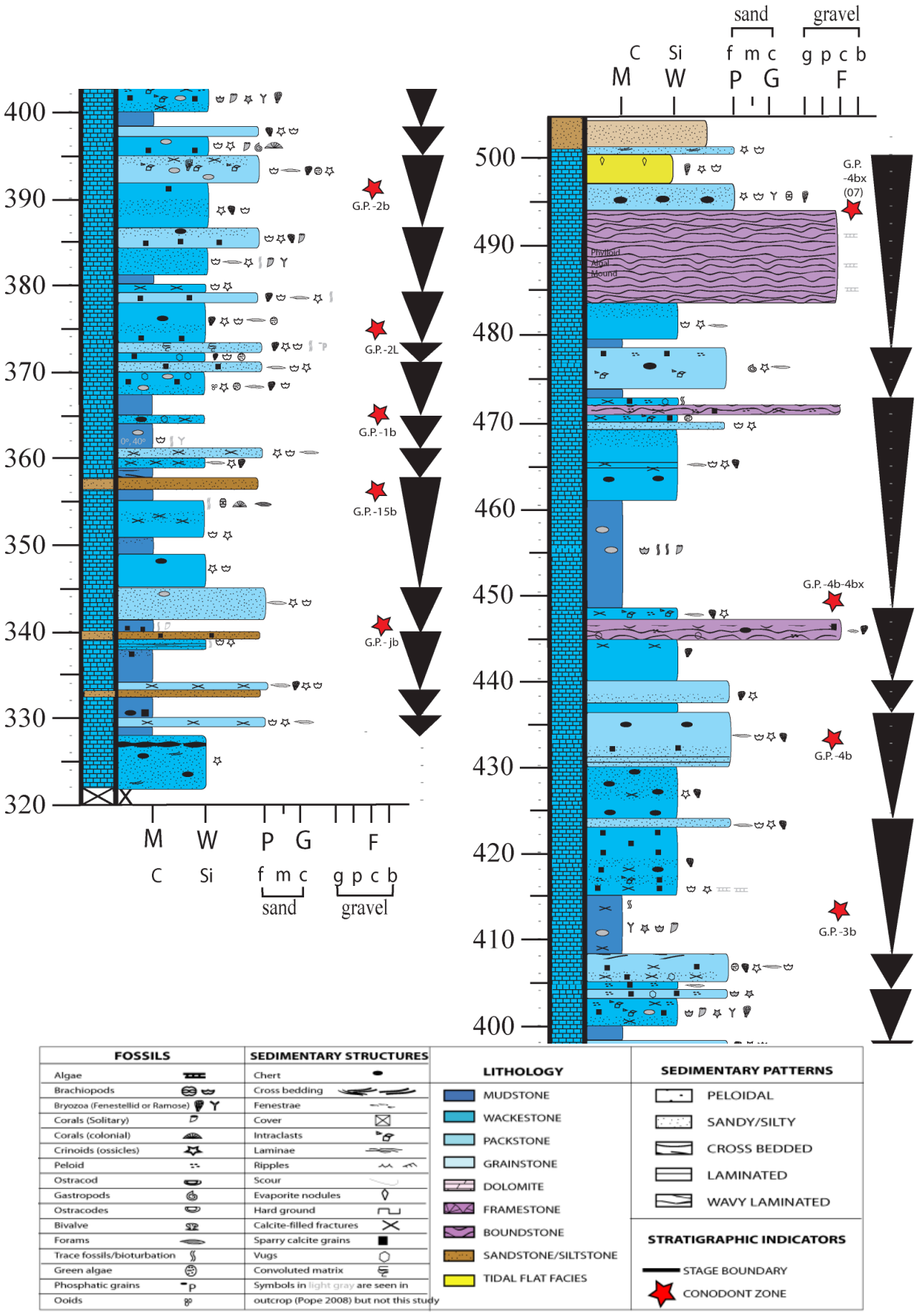

Figure 11: Stratigraphic column for the 328-482 m interval of the Snaky Canyon formation.

Table 1: Lithologic, chemical, and stable isotopic data for Snaky Creek carbonates.

Sample	Lithology[1]	Depth (m)	% CaCO3	Fossil Types					Petrography Features								$\delta^{13}C$ (‰)	$\delta^{18}O$ (‰)
				Crinoid	Bryozoan	Brachiopod	Green algae	Foraminifera	Silt/sand	Fractures	Calcite nodule	Calcite grains	Pellets	Intraclasts	Chert	Other[2]		
1 C	MS	328	90														2.26	-3.73
2 C	PS	329	90	X		X		X										-4.28
3 C	MS	330	50														0.53	-4.62
3 C B	MS	330	60														0.37	-4.41
4 C	MS	331	90									x			x		2.27	-3.48
5 C	SS	332	100						x								1.56	-5.39
6 C	PS	333	100	x	x	x		x	x	x							2.71	-3.73
6 C FRAC	CF	333	100														0.44	-13.86
6 C FRAC B	CF	333	100														0.36	-13.62
7 C	MS	334	60														2.83	-4.97
8 C	MS	335	60														2.10	-4.53
9 C	MS	336	60														2.62	-3.79
9 C B	MS	336	60														2.38	-5.57
10 C	MS	337	80						x			x					2.84	-4.67
11 C	WS	338	90	x					x							l	3.02	-3.54
12 C	SS	339	70						x			x				bu	2.36	-5.38
12 C B	SS	339	70														2.62	-4.89
13 C	MS	340	80								x	x					2.81	-1.03
13 C B	MS	340	80														2.92	-1.04
14 C	MS	341	60														1.77	-4.77
15 C	WS	341.5	90	x		x										m	3.13	-3.39
15 C B	WS	341.5	90														3.11	-3.14
16 C	PS&WS	342	80	x					x							m	2.22	-3.76
17 C	SS	342.5	35						x								1.09	-5.17

Table 1 continued

Sample	Lithology[1]	Depth (m)	% CaCO3	Fossil Types					Petrography Features								$\delta^{13}C$ (‰)	$\delta^{18}O$ (‰)
				Crinoid	Bryozoan	Brachiopod	Green algae	Foraminifera	Silt/sand	Fractures	Calcite nodule	Calcite grains	Pellets	Intraclasts	Chert	Other[2]		
18 C	PS	343	65			x			x							m	-0.71	-8.50
18 C B	PS	343	65														-0.94	-8.76
19 C	PS	343.5	50					x	x							g, bg	1.30	-4.61
20 C	PS	344	35	x					x							g, bg	1.53	-4.79
21 C	PS	345	65					x	x							ws, b	0.98	-4.01
22 C	MS	349	75														0.33	-4.63
22 C B	MS	349	75														0.35	-4.49
23 C	MS	350	80						x								1.43	-4.35
24 C	WS	351	75	x		x			x								1.05	-5.37
25 C	WS	352	60														1.06	-5.15
25 C B	WS	352	60														1.24	-5.16
26 C	WS	353	80						x	x		x					1.78	-3.85
27 C	MS	355	70														-0.71	-6.37
27 C B	MS	355	70														-0.69	-6.34
28 C	MS	356	60														1.87	-4.13
29 C	SS	357	30						x							bg	2.52	-5.01
30 C	MS	358	45						x							bg, g, l	2.69	-4.51
31 C	WS	359	55	x	x			x	x	x							3.32	-5.35
32 C	PS	360	80	x		x		x	x	x							1.71	-5.73
32 C B	PS	360	80														1.78	-4.47
33 C	MS	361	95		x													-4.18
34 C	MS	362	70														0.54	-6.83
34 C B	MS	362	70														0.40	-7.85

Table 1 continued

Sample	Lithology[1]	Depth (m)	% CaCO3	Fossil Types					Petrography Features								$\delta^{13}C$ (‰)	$\delta^{18}O$ (‰)
				Crinoid	Bryozoan	Brachiopod	Green algae	Foraminifera	Silt/sand	Fractures	Calcite nodule	Calcite grains	Pellets	Intraclasts	Chert	Other[2]		
35 C	WS	364	80						x	x					x	v, i	1.92	-7.01
36 C	MS	365	70														1.08	-6.46
37 C	WS	367	80	x					x								2.99	-3.84
38 C	WS	367.5	80														4.02	-3.75
39 C	WS	368	99		x		x	x				x					1.31	
40 C	WS	369	95													v	3.59	-4.15
41 C	PS	370	90	x		x		x	x								3.36	-3.38
42 C	WS	371	95		x	x	x					x					2.76	-6.18
43 C	PS	373	85	x	x	x			x								2.49	-4.38
44 C	WS	374	95		x		x	x				x				m	2.74	
45 C	MS&WS	375	95						x								2.40	-3.76
46 C	WS	377	95	x	x	x		x									2.41	-3.32
47 C	PS&WS	378	95	x	x	x		x				x					2.35	-3.48
48 C	WS	379	100	x	x					x							2.65	-1.97
48 C B	WS	379	100														2.82	-1.69
49 C	MS	380	70														1.76	-3.97
50 C	WS	381	60	x					x								1.68	-4.23
51 C	WS	382	75	x		x		x	x							bg	2.57	-5.53
52 C	WS	383	55	x					x			x				sc	1.85	-6.99
53 C WS	PS	384	60	x	x	x											2.74	-3.69
53 C calc	CN	384	100														-18.90	-2.94
54 C	PS&WS	385	85	x					x						x		2.76	-4.23
55 C	WS	386	90	x	x	x											3.04	-4.31
55 C B	WS	386	90														2.89	-4.98

Table 1 continued

Sample	Lithology[1]	Depth (m)	% CaCO3	Fossil Types					Petrography Features								$\delta^{13}C$ (‰)	$\delta^{18}O$ (‰)
				Crinoid	Bryozoan	Brachiopod	Green algae	Foraminifera	Silt/sand	Fractures	Calcite nodule	Calcite grains	Pellets	Intraclasts	Chert	Other[2]		
56 C	WS	387	60														2.92	-4.38
57 C	WS&MS	388	65		x				x								2.49	-4.01
58 C	WS	389	80		x				x								2.12	-4.77
58 C B	WS	389	80														2.18	-4.96
59 C	WS	390	80														2.88	-1.04
60 C	WS	391	95								x						-0.21	-6.76
60 C B	WS	391	95														-0.16	-6.05
61 C	PS	392	95	x	x			x								bg	3.05	-3.93
62 C	PS	393	98	x	x		x	x						x			3.07	-3.80
63 C	PS&SS	394	90	x	x	x			x	x						bg	2.18	-3.85
63 C B	PS&SS	394	90														2.07	-3.92
64C CALC	CN	395	100								x							
64 C VF	WS	395	95	x							x						1.33	-6.84
64 C VF B	WS	395	95														1.05	-6.86
65 C	WS	396	95	x		x										sb	-0.01	-7.32
65 C B	WS	396	95														-0.28	-7.05
66 C	PS	397	98	x		x		x									3.02	-3.86
67 C	MS	398	90														2.92	-4.15
68 C	MS	399	90														0.79	-8.62
68 C B	MS	399	90														0.76	-8.32
68 C C	MS	399	90														0.52	-8.45
69 C	WS	400	85						x	x							1.81	-5.22
70 C	WS	401	98									x		x			4.60	-4.64
71 C	WS	402	99							x		x	x				4.17	-6.76

Table 1 continued

Sample	Lithology[1]	Depth (m)	% CaCO3	Fossil Types					Petrography Features								$\delta^{13}C$ (‰)	$\delta^{18}O$ (‰)
				Crinoid	Bryozoan	Brachiopod	Green algae	Foraminifera	Silt/sand	Fractures	Calcite nodule	Calcite grains	Pellets	Intraclasts	Chert	Other[2]		
72 C	PS	403	97									x	x			v, gy	4.82	-4.42
73 C	WS	404	99					x		x		x	x				4.37	-3.42
74 C	PS	405	93	x				x	x	x		x				v, gy	3.73	
74 C B	PS	405	93														3.84	-5.28
75 C	PS	406	99	x			x	x		x		x					4.38	-2.88
76 C	PS	407	95	x	x	x		x								st	3.51	-3.71
77 C	MS	408	90							x								
77 C FRAC	CF	408	100	-						x							3.26	
78 C	MS	409	70														3.63	-3.50
79 C	MS	410	70	-													3.55	-3.97
80 C	MS	411	65	-													3.75	-3.09
81 C	MS	412	60							x							3.56	-3.99
81 C FRAC	CF	412	100							x							3.62	-4.61
82 C	MS	413	95														3.82	-4.70
82 C B	MS	413	95														3.78	-3.99
83 C	MS	414	70														3.20	-5.26
84 C	WS	415	99							x		x					3.66	-4.96
85 C WS	WS	416	95						x			x	x	x		st	1.88	-6.29
85 C MS	PS	416	95														3.56	-4.23
86 C	WS	417	100							x							3.43	-4.86
87 C	WS	418	65		x				x								0.91	-6.24
88 C	WS	419	98	-								x					0.01	-7.79
88 C B	WS	419	98	-													0.06	-7.60
88 C C	WS	419	98														-0.07	-7.33

Table 1 continued

Sample	Lithology[1]	Depth (m)	% CaCO3	Fossil Types					Petrography Features								$\delta^{13}C$ (‰)	$\delta^{18}O$ (‰)
				Crinoid	Bryozoan	Brachiopod	Green algae	Foraminifera	Silt/sand	Fractures	Calcite nodule	Calcite grains	Pellets	Intraclasts	Chert	Other[2]		
89 C	WS	420	90		x							x					2.10	-6.96
89 C B	WS	420	90														1.71	-5.97
90 C	WS	421	98		x							x					1.39	-5.98
90 C B	WS	421	98														1.28	-5.87
92 C	PS	423	70	x	x	x		x	x								2.44	-4.16
95 C	WS	426	95		x										x		1.41	-6.83
95 C B	WS	426	95														1.42	-5.48
96 C	WS	427	50	x					x						x	cc	2.75	-1.52
97 C	WS	428.5	45	x					x			x			x	cc, l	2.85	-2.37
98 C	PS	430	85	x	x	x			x							l, i, py	1.92	-5.63
98 C B	PS	430	85														1.86	-5.24
89 C	WS	420	90		x							x					2.10	-6.96
89 C B	WS	420	90														1.71	-5.97
90 C	WS	421	98		x							x					1.39	-5.98
90 C B	WS	421	98														1.28	-5.87
92 C	PS	423	70	x	x	x		x	x								2.44	-4.16
95 C	WS	426	95		x										x		1.41	-6.83
95 C B	WS	426	95														1.42	-5.48
96 C	WS	427	50	x					x						x	cc	2.75	-1.52
97 C	WS	428.5	45	x					x			x			x	cc, l	2.85	-2.37
98 C	PS	430	85	x	x	x			x							l, i, py	1.92	-5.63
98 C B	PS	430	85														1.86	-5.24
99 C	PS	431.5	85	x	x	x			x			x					2.68	-4.45

Table 1 continued

Sample	Lithology[1]	Depth (m)	% CaCO3	Fossil Types					Petrography Features								$\delta^{13}C$ (‰)	$\delta^{18}O$ (‰)
				Crinoid	Bryozoan	Brachiopod	Green algae	Foraminifera	Silt/sand	Fractures	Calcite nodule	Calcite grains	Pellets	Intraclasts	Chert	Other[2]		
100 C	PS	433	95	x	x			x									2.52	-4.31
101 C PS1	PS	434.5	90	x				x							x		1.94	-6.12
101 C PS1 B	PS	434.5	90														2.21	-4.08
101 C PS2	PS	434.5	90	x				x							x		2.06	-3.97
101 C PS2 B	PS	434.5	90														1.57	-4.41
102 C	WS	436	90														1.50	-5.89
102 C B	WS	436	90	-													1.56	-5.99
102 C C	WS	436	90	-													1.52	-5.64
103 C	PS	437	80	x	x				x							sc	2.45	-4.91
106 C	WS	440	90														2.65	-2.42
106 C B	WS	440	90														2.72	-2.38
107 C	WS	441	90														0.93	-6.80
107 C B	WS	441	90														0.96	-6.40
107 C C	WS	441	90														0.93	-6.40
108 C	WS	442	90	-													2.89	
108 C B	WS	442	90														3.08	-2.58
109 C	WS	443	90														2.91	-3.69
110 C	WS	444	90	-	x					x							2.17	-5.17
111 C	BS	446	90		x							x	x		x	v	3.40	-3.45
112 C	WS	447	95	x	x	x		x		x			x	x			3.66	-3.72
113 C	MS	448	90														2.63	-3.90
114 C	MS	449	90														3.08	-3.43
100 C	PS	433	95	x	x			x									2.52	-4.31
101 C PS1	PS	434.5	90	x				x							x		1.94	-6.12

Table 1 continued

Sample	Lithology[1]	Depth (m)	% CaCO3	Fossil Types					Petrography Features								$\delta^{13}C$ (‰)	$\delta^{18}O$ (‰)
				Crinoid	Bryozoan	Brachiopod	Green algae	Foraminifera	Silt/sand	Fractures	Calcite nodule	Calcite grains	Pellets	Intraclasts	Chert	Other[2]		
101 C PS1 B	PS	434.5	90														2.21	-4.08
101 C PS2	PS	434.5	90	x				x							x		2.06	-3.97
101 C PS2 B	PS	434.5	90														1.57	-4.41
102 C	WS	436	90														1.50	-5.89
102 C B	WS	436	90	-													1.56	-5.99
102 C C	WS	436	90	-													1.52	-5.64
103 C	PS	437	80	x	x				x							sc	2.45	-4.91
106 C	WS	440	90														2.65	-2.42
106 C B	WS	440	90														2.72	-2.38
107 C	WS	441	90														0.93	-6.80
107 C B	WS	441	90														0.96	-6.40
107 C C	WS	441	90														0.93	-6.40
108 C	WS	442	90	-													2.89	
108 C B	WS	442	90														3.08	-2.58
109 C	WS	443	90														2.91	-3.69
110 C	WS	444	90	-	x					x							2.17	-5.17
111 C	BS	446	90		x							x	x		x	v	3.40	-3.45
112 C	WS	447	95	x	x	x		x		x			x	x			3.66	-3.72
113 C	MS	448	90														2.63	-3.90
114 C	MS	449	90														3.08	-3.43
115 C	MS	453	85															-5.39
116 C	MS	454	75														3.02	-4.60
117 C	MS	455	80														2.26	-4.77
118 C	MS	456	85														3.05	-5.63

Table 1 continued

Sample	Lithology[1]	Depth (m)	% CaCO3	Fossil Types					Petrography Features								$\delta^{13}C$ (‰)	$\delta^{18}O$ (‰)
				Crinoid	Bryozoan	Brachiopod	Green algae	Foraminifera	Silt/sand	Fractures	Calcite nodule	Calcite grains	Pellets	Intraclasts	Chert	Other[2]		
119 C	MS	457	90														0.66	-6.93
119 C B	MS	457	90														0.64	-7.14
120 C	MS	458	85														3.87	-4.18
121 C	MS	459	85														3.92	-4.27
122 C	MS	460	90														3.72	-4.47
123 C	MS	461	90														3.29	-4.17
124 C	WS	462	85														2.81	-4.99
125 C	WS	463	85	x	x			x							x		3.17	-1.97
126 C	WS	464	90														3.17	-1.92
127 C	WS	465	95	x	x	x				x						sb, l	1.80	-6.13
127 C B	WS	465	95														1.57	-5.94
130 C	WS	468	90	x					x								2.34	-7.60
130 CB	WS	468	90														2.00	-7.40
131 C	PS	469	70	x		x			x							g	3.32	-3.87
132 C	WS	470	80				x			x		x	x				3.75	-4.79
133 C	BS	471	99							x		x	x				3.83	-5.25
134 C	WS	472	98							x		x	x			bu, d	3.26	-6.37
135 C	MS	473	90														3.87	-5.48
136 C	PS	474	99					x						x			4.46	-4.29
137 C	PS	475	97	x												bg, sc	3.90	
139 C	PS	477	98					x				x	x				3.59	-6.03
140 C	MS	478	90														3.74	-5.76
142 C WS	WS	480	90														4.30	-4.98
142 C PS	PS	480	90														4.35	-5.05

Table 1 continued

Sample	Lithology[1]	Depth (m)	% CaCO3	Fossil Types					Petrography Features								$\delta^{13}C$ (‰)	$\delta^{18}O$ (‰)
				Crinoid	Bryozoan	Brachiopod	Green algae	Foraminifera	Silt/sand	Fractures	Calcite nodule	Calcite grains	Pellets	Intraclasts	Chert	Other[2]		
142 C PS	PS	480	90														4.35	-5.05
143 C	WS	481	97	x		x		x								sc	4.04	-4.93
144 C	WS	482	85	x		x											2.16	-7.80
144 C B	WS	482	85														2.26	

[1]CF = calcite fraction, CN = calcite nodule, BS = boundstone, GS = grainstone, MS = mudstone, PS = packstone, WS = wackestone, SS = sandstone.

[2]b = biogenic, bg = biogenic grain, bu = burrows, cc = chert cement, d = dolomite, g = grading, gy = gypsum, i = iron, l = laminated, m = micritized, p = pyrite, sb = silicified brachiopod, sc = silicified crinoid, st = stylolite, v = vuggy, ws = well sorted

.

Grossman, E. L., 1999. Oxygen Isotopes, in The Encyclopedia of Geochemistry, Marshall, C.P. and Fairbridge R.W., eds., p. 469-474.

Grossman, E.L., 2002, Stable carbon isotopes as indicators of microbial activity in aquifers, *in* Manual of Environmental Microbiology, 2nd ed., C.J. Hurst et al. (eds.), American Society for Microbiology Press, Washington, DC, p. 728-742

CONTACT INFORMATION

Name:	Stephanie G. Wood
Professional Address:	c/o Dr. Ethan Grossman Geology and Geophysics Department MS 3115 Texas A&M University College Station, TX 77843
	c/o Dr. Mike Pope Geology and Geophysics Department MS 3115 Texas A&M University College Station, TX 77843
Email Address:	stephanie.wood11@gmail.com
	e-grossman@geos.tamu.edu
	mcpope@geo.tamu.edu
Education:	B.S., Geology, Texas A&M University, May 2011 Undergraduate Research Scholar